Chapter 2

Experiment and simulation

2.1 Introduction

Nuclear emulsion is a dispersion of silver halide crystals in a gelatin matrix. The medium is used to record charged particle tracks of silver halide micro-crystals fixed into about equal parts in volume, a matrix material consisting of gelatin and water with a small amount of glycerol and a few other substances. An electrically charged particle while passing through the medium produces a latent image. Under proper chemical treatment the image appears as trails of black colloidal grains of metallic silver along the trajectory of the particle. The photo-sensitive silver halide material (mostly AgBr) has three to four times more concentration in nuclear emulsion than that in a conventional photographic plate. The AgBr grains in nuclear emulsions are well separated and are much smaller in size (less than a micron in diameter), whereas the AgBr grains in an ordinary photographic plate are interlocked and they can be as large as several microns. The Ilford G5 emulsion plates used in this experiment have a grain diameter of about 0.3 micron. However, the mean crystal grain diameters are different in different types of emulsions. It is observed that the contrast of nuclear emulsion may be improved if the grains are uniform in size, and the sensitivity goes up with increasing grain size. The dimension of each Ilford G5 emulsion pellicle used in the present investigation is 18 cm. $\times$ 7 cm. $\times$ 600 microns. Gelatin being a hygroscopic material, emulsion can absorb water from the atmosphere. Therefore, while citing the relative size and composition of emulsions, it is necessary to mention the *shrinkage factor* of

Table 2.1: Chemical composition of standard emulsion.

Element	Atomic weight (A)	No. of atoms per cc $\times 10^{20}$	Moles per cc $\times 10^{-3}$	Concentration at 58% R.H.
I	129.93	0.565	0.094	0.012
Ag	107.88	101.01	16.764	1.817
Br	79.92	100.41	16.673	1.338
S	32.06	1.353	0.216	0.249
O	16.0	94.97	16.050	0.007
N	14.01	31.68	5.147	0.053
C	12.0	138.30	22.698	0.227
H	1.008	321.56	53.571	0.074

the medium, and the real time relative humidity of the surrounding. The chemical composition of a standard research emulsion (such as Ilford G5) is given in Table 2.1. In emulsion the total number of atoms is 7.898×10^{22} per cc, whereas the total number of electrons is 1.0446×10^{24} per cc. Taking the nuclear radius parameter $r_0 = 1.2$ fm, the geometrical mean free path of all the elements present in nuclear emulsion comes out ≈ 37 cm. However, the actual interaction mean free path is quite different from this geometrical value.

2.2 Properties of emulsion tracks

The nature of a track formed within emulsion medium depends upon the particle type, energy etc. For instance, a high velocity/energy particle will create rarer grain density that leads to a thinner track. A comprehensive description of the development of tracks created by charged particles in nuclear photo-emulsion is given in [1]. Here we briefly describe some of the important features of the tracks formed in nuclear emulsions.

(a) **Grain density:** The development of grains in emulsion takes place due to the energy lost by charged particles through ionization while passing through the medium. The grain density is measured to characterize lowly ionizing and fast moving charged particles. The number of grains deposited per micron of a track is defined as the grain density, which is proportional to, (i) the rate of energy lost by the moving particle dT/dx (in KeV per micron), and (ii) the square of the charge (Z) of the particle. A relationship between the grain density dn/dx and the rate of energy loss dT/dx like

$$\frac{dn}{dx} = c\left[1 - \exp\left\{b\,Z\left(\frac{dT}{dx}\right)^{1/2} - a^{1/2}\right\}\right] \tag{2.1}$$

has been experimentally verified [2]. Here a, b and c are empirical constants. Consequently, the grain density will have a maximum value near the end of the track. It was found that, as the velocity (β) of charged particle increases, the corresponding grain density initially decreases and reaches a minimum at $\beta \approx 0.45$, and then it saturates slightly above the least value [3–6]. The rise in grain density above the minimum value is due to the distortion of the field associated with the particle – an increase in velocity leads to the longitudinal contraction and lateral extension of the field of the moving particle [1]. The rate of energy loss is found to be $\delta E \sim \log E$. However, this is not reflected in the grain density, as the energy dissipation mostly takes place outside the core of the track. Nevertheless, some of the additional energy loss may lead to the formation of the so-called δ rays, which contribute to the observed limited increase in the grain density. The Cerenkov radiation also contributes to the grain density. Gelatine which has a refractive index ≈ 1.5 will be a source of Cerenkov radiation when $\beta > 2/3$ [7]. Sometimes instead of grain density, the blob density B is measured. A blob is a resolvable spot in which more than one grains are present. The estimation of blob number is equivalent to measuring the number of gaps between two blobs. It is observed that the frequency distribution of gap length exponentially decreases with increasing gap length [8]. The number density of the gaps H exceeding a gap-length l is given by [9]

$$H = B \exp(-g\, l) \tag{2.2}$$

The slope parameter g is a measure of grain density, but is not exactly equal to the grain density dn/dx. Fowler and Perkins gave an alternative relation for the blob density [9]

$$B = g \exp(-g\, \alpha) \tag{2.3}$$

where α is a parameter determined by the average grain size. From these two relations one can determine g as a useful ionizing parameter.

(b) **Lacunarity and opacity:** The lacunarity of a track

$$L = \int_0^\infty -l \left(\frac{dH}{dl}\right) dl = \exp\left(-g\, \alpha\right) \tag{2.4}$$

is defined as the fraction of the track made up of gaps. From Equation (2.3) and Equation (2.4) we get, $g = B/L$ and $\alpha = -(L/B) \ln L$. For particles with low Z and high velocity ($\beta \sim 1$) the specific energy loss is small. In such cases the following proportionality holds

$$\frac{dE}{dx} \propto \frac{dn}{dx} \tag{2.5}$$

Assuming $g \propto dn/dx$, one may get $Z^2 \propto -\ln L$. Opacity $\mathcal{O}$ on the other hand, is defined as the fraction of a track that is made up of blobs, and therefore it is related to lacunarity as $\mathcal{O} = 1 - L$. The charge of the track forming particle can be determined either by measuring its lacunarity or opacity. By default for low Z ($Z = 2 - 3$), a high degree of accuracy for the charge measurement can be achieved in this method, because of a dependence like

$$\delta Z \propto \frac{1}{Z}\frac{\delta L}{L} \tag{2.6}$$

Here the error $\delta L = \sigma_L/\sqrt{N_c}$ can arbitrarily be reduced by increasing N_c, the number of cells of equal length over which the measurement of L has been made, and $\sigma_L = \sqrt{\langle L^2\rangle - \langle L\rangle^2}$ is the variance in L.

(c) **Delta-rays:** For large Z the rate of energy loss of the moving particle is high, and secondary electrons are produced with sufficient kinetic energies. Some of these electrons may have observable tracks within emulsion. Such electron tracks are referred to as δ-rays. The number of delta-rays n_δ per unit length depends on the specific energy loss as,

$$-\frac{dE}{dx} = \frac{4\pi e^4\, Z_p^2 N Z_t}{mv^2}\left[\ln\left(\frac{2mv^2}{I}\right) - \ln(1-\beta^2) - \beta^2\right] \tag{2.7}$$

where N is the number of atoms per unit volume of the emulsion material, Z_t and I are respectively, the mean atomic number and ionization potential of the emulsion nuclei and Z_p is the projectile charge number. Therefore, when the lacunarity measurement is not permitted, the method of delta ray counting can be utilized to determine the charge of a particle. For a particle of charge Ze the number of delta rays with energies between W and $W + dW$ is given by [10, 11],

$$dn_\delta = \frac{2\pi N Z_p^2 e^4}{m_e v^2}\frac{dW}{W}\left[1 - \beta^2\frac{W}{W_{\max}}\right] \tag{2.8}$$

where the upper limit of energy that the electron may receive is

$$W_{\max} = \frac{2m_e v^2\gamma^2}{1 + 2\gamma\frac{m_e}{m} + (\frac{m_e}{m})^2} \tag{2.9}$$

and $\gamma = 1/\sqrt{1-\beta^2}$ is the Lorentz factor. The lower limit of delta-ray energy is approximately 10 KeV. Integrating Equation (2.8) we get $n_\delta \propto Z^2/\beta^2$. This formula can be utilized to determine the charge of the particle.

(d) **Particle range:** Charged particles loose energy through collisions with the atoms present in the medium through which they traverse. When the energy of the moving particle becomes less than the ionization potential of the atoms present in the medium, the particle in motion suffers multiple elastic scattering and ultimately stops within

the medium. The track length of the particle is the distance along the trajectory starting from its point of origin to the last developed grain. It is also known as the residual range (R). The true range can then be defined as the distance traveled by the particle before it stops within the emulsion. Knowing the specific energy loss dE/dx and initial energy E_0, the range of a particle can be determined from the following formula,

$$R(E_0) = \int_0^{E_0} \frac{1}{dE/dx} dE \tag{2.10}$$

Using Equation (2.7) we get from the above

$$R(E_0) = \frac{m}{Z^2} f(v_0) \tag{2.11}$$

where $f(v_0)$ depends only on the initial velocity v_0. In the non-relativistic limit ($E_0 \ll mc^2$) a range-energy relation for any particle is similar to that of a proton, $R_p = K\, E_p^n$, where R_p is in microns and the kinetic energy E_p is in MeV, $K \approx 0.262$ and $n \approx 0.575$ are experimentally obtained parameters. For a particle of mass m and charge Ze the range-energy relation reads as [12],

$$E = K \left(\frac{m}{m_p}\right)^{(1-n)} Z^{2n} R^n \tag{2.12}$$

where m_p is the rest mass of proton. Due to different statistical effects, ranges of even mono-energetic particles exhibit straggling. A straggling parameter is defined as,

$$\Gamma_R = \frac{\pi}{2} \left[\frac{\sum_{i=1}^{N} (R_i - \overline{R})^2}{N}\right]^{1/2} \tag{2.13}$$

The FWHM (ΔR) of the differential range distribution is related to Γ_R by $\Delta R = 0.94\Gamma_R$.

(e) **Track width:** For a highly ionizing particle the linear track structure contains little information in terms of grain or blob density as n_δ becomes too large to count [13]. In those cases the track width is a useful parameter to identify the charge of a particle. The track width depends on various factors. For instance, the type of emulsion and the developer used, the particle charge, its mass, velocity etc. Experimentally it is found that the track width increases linearly with Z (for $Z > 10$). As the track caused by a heavy-ion reaches toward its end, a thinning down (tapering) of the track is observed due to electron capture, which reduces the effective charge of the ion. The length of this tapered portion (L_t) of the track may also be used to find out the atomic number

of the particle [14]. The following empirical relation is obtained in this regard,

$$L_t \sim Z^{\nu}, \qquad \text{where} \;\; \nu \approx 1.0 \tag{2.14}$$

(f) **Shrinkage factor:** Gelatin and glycerin are both hygroscopic materials. The actual equilibrium thickness and refractive index of both processed and unprocessed emulsion depends on the surrounding humidity. For a qualitative measurement of the track densities, range and angles in emulsion, the original thickness of the emulsion has to be known. The shrinkage factor of emulsion is a parameter that relates the actual thickness of the emulsion plate with its measured thickness. The shrinkage factor S, generally supplied by the manufacturer, is defined by

$$S = \frac{\text{thickness of emulsion layer during exposure}}{\text{thickness of emulsion layer during scanning}} \tag{2.15}$$

2.3 Scanning of emulsion plates

Scanning of an emulsion plate is performed by using along-the-track method under the view of the microscopes. Two different scanning methods are generally employed.

(a) **Area or volume scanning:** In an area scanning the focal surface of an emulsion plate is swept up and down from the surface of an emulsion to the supporting glass plate. This is done by rolling the fine focus control while observing the events successively coming into and going out of view. Each field of view is scanned from one surface of the emulsion to the other. That means a definite area (actually a volume) of the plate is scanned. Area scanning is employed under the following circumstances, (i) when the events of a particular type in a given volume are to be found, and (ii) when the situation demands a representative sample. Preliminary volume or line scanning may be performed under a magnification of $300 - 400\times$, but the angle measurement and track identification should finally be done under a higher magnification ($\gtrsim 1000\times$). The area scanning however is not an efficient method to find out the single diffractive dissociation events, interactions with the hydrogen nuclei, and therefore to build up a minimum bias event sample.

(b) **Along the track scanning:** If a stack of emulsion pellicles is exposed to a beam of particles, or if one wishes to study the density and distribution of the beam tracks in the stack, then the procedure for finding the tracks is to traverse each plate parallel to the leading edge and perpendicular to the incoming tracks. This type of scanning is known as *along the track scanning*. The scanning operation is often tiresome and

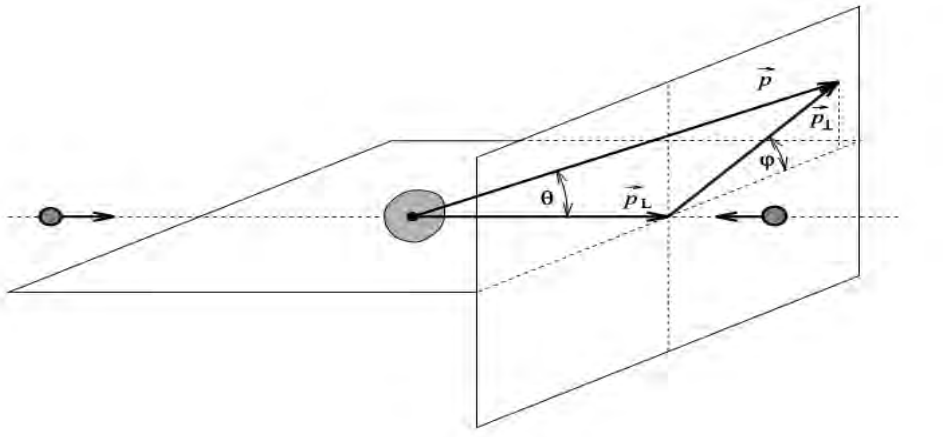

Figure 2.1: Schematic of a secondary track geometry with respect to the projectile.

time consuming. It requires a lot of concentration on the part of the scanner, and the experimental results depend largely upon the correct decision. Care should be taken to avoid personal bias and subjectivity in the decision. To avoid individual bias, the same data sample may be counter checked by independent observers. Electronic counting will no doubt be a faster process, but it would not be an intelligent method of scanning. Like in the case of area scanning, the preliminary scanning along the track may be performed under a magnification of $300 - 400\times$, though the final selection of events has to be done under a higher magnifications ($\sim 1000\times$). By adopting the along the track scanning method it is possible to build up a sample of minimum bias events in emulsion experiments.

2.4 Measurement methods

(a) **Counting and statistics:** Nuclear-emulsion can discriminate between various types of events as well as tracks originating from different types of events. The ionization of a track may be measured by counting the number of grains or blobs over a particular segment of the track (say 100 μm of length). Delta-rays over a similar length interval may be counted to identify the charge of the particle producing the track. Energy spectra are determined by counting the number of tracks within a particular range interval. Angular distributions are determined by counting the number of tracks within the prescribed angular intervals. In order to establish the reliability of the collected data, a practical knowledge of counting statistics is therefore required. The track geometry is schematically presented in Figure 2.1. In high-energy interactions often a large number $(10^2 - 10^3)$ of new particles are produced. The resulting tracks come out from the interaction vertex within a narrow forward angular interval. Often it becomes

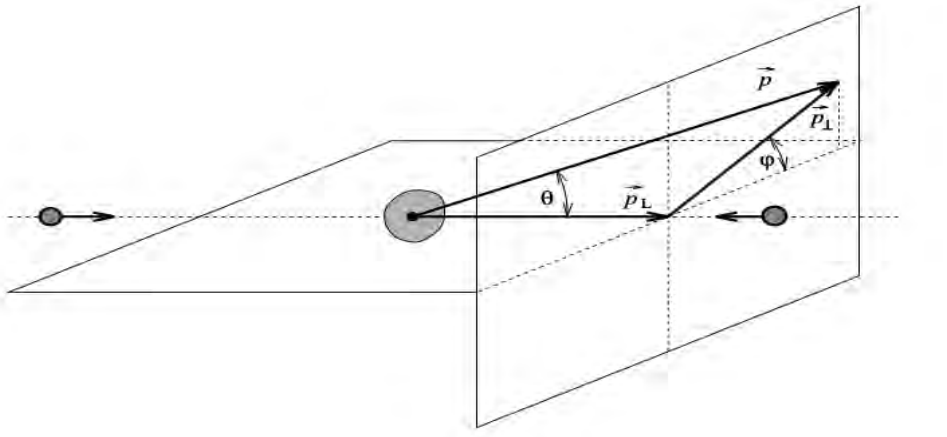

Figure 2.1: Schematic of a secondary track geometry with respect to the projectile.

time consuming. It requires a lot of concentration on the part of the scanner, and the experimental results depend largely upon the correct decision. Care should be taken to avoid personal bias and subjectivity in the decision. To avoid individual bias, the same data sample may be counter checked by independent observers. Electronic counting will no doubt be a faster process, but it would not be an intelligent method of scanning. Like in the case of area scanning, the preliminary scanning along the track may be performed under a magnification of $300 - 400\times$, though the final selection of events has to be done under a higher magnifications ($\sim 1000\times$). By adopting the along the track scanning method it is possible to build up a sample of minimum bias events in emulsion experiments.

2.4 Measurement methods

(a) **Counting and statistics:** Nuclear-emulsion can discriminate between various types of events as well as tracks originating from different types of events. The ionization of a track may be measured by counting the number of grains or blobs over a particular segment of the track (say 100 μm of length). Delta-rays over a similar length interval may be counted to identify the charge of the particle producing the track. Energy spectra are determined by counting the number of tracks within a particular range interval. Angular distributions are determined by counting the number of tracks within the prescribed angular intervals. In order to establish the reliability of the collected data, a practical knowledge of counting statistics is therefore required. The track geometry is schematically presented in Figure 2.1. In high-energy interactions often a large number $(10^2 - 10^3)$ of new particles are produced. The resulting tracks come out from the interaction vertex within a narrow forward angular interval. Often it becomes

very difficult to distinguish one track from the other. The problem is more profound in the forward direction of an event, that is densely populated by jets of particles. In such cases one may have to take help of a nearby projectile track located within the same field of view, that is essentially moving parallel to the projectile track under consideration. It is to be noted that if the projectile tracks are close to each other, they will experience almost identical distortions in the emulsion. Heavy-ion interactions are rich sources of highly energetic photons. These photons may interact with the Coulomb/nuclear field(s) available in the emulsion medium, and produce e^-e^+ pairs. The angular separations between the electron and positron tracks are often very small, and therefore it is often extremely difficult to identify them as two separate tracks. Moreover, if the $\gamma \rightarrow e^-e^+$ conversion takes place near the interaction vertex, it is very likely that the e^-e^+ tracks will be confused with tracks originating from the primary interaction vertex. When the coordinates of points are recorded at a large distance from a particular interaction vertex, there may be interference with the tracks coming from other interactions as well. These problems can be solved by recording the coordinates of several points on a single track, and through a reconstruction program one may obtain the best fitted track. One may also extrapolate the fit to check whether the straight line is passing through the coordinates of the interaction vertex or not.

(b) **Dip angle:** The dip angle ξ of a straight track is defined as,

$$\tan\xi = \Delta z/L \tag{2.16}$$

where Δz is the true difference of depth between any two points on the track and L is the length of the projection of the track between these two points. If dry objectives are used, the apparent depth d_a will be less than the corresponding true depth ($d_t = \mu_e\, d_a$). For oil-immersion objectives d_a and d_t are more or less equal because the refractive index of the immersion oil is roughly equal to that of the emulsion medium, $\mu_{\rm oil} \approx \mu_{\rm emul} = 1.52$. The true dip angle ξ_t at the time of passage of the particle is then given by

$$\tan\xi_t \;=\; S\tan\xi \;=\; S\Delta z/L \;=\; S\mu\,\Delta z/L \tag{2.17}$$

where S is the shrinkage factor.

(c) **Space angle:** The space angle or the emission angle θ of a track with respect to the beam direction, may also be measured by a simple coordinate method. If two tracks are characterized by their direction cosines (l_1, m_1, n_1) and (l_2, m_2, n_2), then θ is given by,

$$\cos\theta = l_1l_2 + m_1m_2 + n_1n_2 \tag{2.18}$$

The direction cosine of a track is related to the spatial coordinates of two pints on the track (x_1, y_1, z_1) and (x_2, y_2, z_2) by the relation

$$l = \frac{(x_2 - x_1)}{d};\ m = \frac{(y_2 - y_1)}{d};\ n = \frac{(z_2 - z_1)}{d} \tag{2.19}$$

for $d = [(x_2 - x_1)^2 + (y_2 - y_1)^2 + (z_2 - z_1)^2]^{1/2}$. In order to find out the emission angle of a secondary track one needs to find out the direction cosines of the track as well as the direction cosines of the projectile track.

(d) **Azimuthal angle:** The azimuthal plane of an interaction is defined as a plane perpendicular to the direction of motion of the projectile nucleus. The track direction projected in this plane with respect to some reference direction may be defined as the azimuthal angle φ of a track (measured counter clockwise). If the projectile direction coincides with one of the directions of the horizontal stage movement (say the x-direction), then

$$\varphi = \tan^{-1}\left(\frac{S\Delta z}{\Delta y}\right) \tag{2.20}$$

If the projectile direction does not completely coincide with the x-direction of the stage motion, then φ for the track is measured by setting the corresponding quantity for the projectile track to zero.

(e) **Range measurement:** Due to scattering the track of a charged particle in emulsion may not always be straight. The particle under consideration may deviate from its original direction due to Coulomb scattering. Therefore, it is convenient to break up a track into M number of linear segments, and the residual range of the particle may be determined from the relation,

$$R = \sum_{i=1}^{M}[(x_i - x_{i-1})^2 + (y_i - y_{i-1})^2 + S^2(z_i - z_{i-1})^2]^{1/2} \tag{2.21}$$

where S is the shrinkage factor along the vertical direction. For mounted plates generally no shrinkage factor is associated along the horizontal directions.

(f) **Momentum measurement:** While passing through the emulsion medium, charged particles experience frequent small deflections due to elastic scatterings effected by the Coulomb field of the atomic nuclei present in the medium. According to [15], the mean projected absolute angle of deviation Θ is given by,

$$\bar{\Theta} = \frac{k\,Z}{p\,\beta}\left(\frac{t}{100}\right)^{1/2} \tag{2.22}$$

Here t is the track length followed, Z is the average atomic number of nuclear emulsion, and k is the scattering constant given by,

$$k = e^2 \, Z \, Z_p \, N^{1/2} \left[\ln \left(\frac{\phi_1}{\phi_2} \right) \right]^{1/2} \tag{2.23}$$

N is the number of atoms per unit volume in emulsion, Z_p is the atomic number of the particle moving with velocity $\beta = v/c$ and momentum p, and ϕ_1 (ϕ_2) is the maximum (minimum) value of the projected angle in the plane of the particle trajectory. For an accurate measurement of $\bar{\Theta}$ one can follow the procedure outlined in [16]. Accordingly, the plate is placed on a mechanical stage in such a way that the track is approximately parallel to one of the sides of the stage, say the x-direction. The coordinate (x_0, y_0) of an arbitrary point on the track is measured. The plate is then displaced by a distance t along the x-direction, and the ordinate y_1 of the point is determined by means of an eye-piece scale. The measurement should be performed under a very high magnification ($> 1500\times$), and the ordinate eye-piece scale is commonly replaced by a flair micrometer, which is capable of reading distances within a few hundreds of micron. Once again the stage is moved through the standard distance t, and the ordinate y_2 is recorded. The operation is repeated several times along the length of the track. The absolute value of the second differences, $D_i = |y_{i+2} - 2y_{i+1} + y_i|$ of successive such measurements are determined. The mean absolute value of the second difference between successive chords of length t, corrected for the stage noise and cell length, $\bar{D} = \sum_i^n D_i/n$, can be used to find out $\bar{\Theta}$,

$$\bar{\Theta} = \left(\frac{180}{\pi} \right) \left(\frac{\bar{D}}{t} \right) \tag{2.24}$$

From Equation (2.22) and Equation (2.24) one can determine $p\,\beta$. It is assumed that the energy loss in a given cell length t of the track is negligible.

2.5 Data characteristics

The data used in this investigation are obtained from the stacks of Ilford G5 nuclear emulsion plates horizontally irradiated by the ^{16}O beam at an incident momentum $p_{\rm lab} = 200$ GeV/c per nucleon. The equivalent CM energy is $\sqrt{s_{NN}} = 20.05$ GeV. The experiment (EMU-08) was performed at the Super-proton Synchrotron (SPS) of CERN by the SUNY at Buffalo group [17]. ^{16}O-emulsion events are found by adopting along the track scanning method

using Leitz microscopes under a total magnification 300×. The angle measurements, categorization and counting of tracks etc. are performed by using Koristka microscopes under a magnification 1500×.

2.5.1 Event selection

To reduce the loss of tracks and minimize the errors in angle measurements, we exclude events found within 20μm thickness from either the top or bottom surface of the plates and events found within 1 mm from the edges of the plates. Proper care was taken to discard interactions induced by the secondary tracks. Using along the track scanning method the total path length followed for ^{16}O-projectile tracks was 117.19 mt. Total number of inelastic ^{16}O+emulsion events found within this path length was 1070. Out of these 957 were inelastic collisions with the emulsion nuclei and 113 were electromagnetic dissociation events [18]. The mean free path for nuclear interactions was $\lambda_{\rm nucl} = 12.25 \pm 0.40$ cm and that for the electromagnetic dissociation events was $\lambda_{\rm ED} = 103.71 \pm 9.76$ cm. Corresponding interaction cross-sections were $\sigma_{\rm nucl} = 1033 \pm 38$ mb. and $\sigma_{\rm ED} = 592 \pm 57$ mb. respectively. The corresponding numbers for the ^{32}S-projectile can be found elsewhere [19].

2.5.2 Track classification

The tracks emitted from an interaction are classified into the following categories.

1. **Shower tracks:** The shower tracks are produced by singly charged particles moving with speed $\beta > 0.7$. The shower tracks comprise mostly of charged pions with a few percent admixture of charged kaons. The shower tracks have an ionization $I \leq 1.4 I_0$, where I_0 is the minimum ionization due to any track observed within the emulsion plate. The multiplicity of such tracks in an event is denoted by n_s.

2. **Gray tracks:** The gray tracks are generally produced by the protons that directly participate in an interaction and are knocked out from the target nuclei. The energy range of gray tracks is usually $30-400$ MeV. The ionization of gray tracks lies between $1.4\,I_0$ and $10\,I_0$. In nuclear emulsion their range exceeds 3 mm. The velocity range of these particles is $0.3c$ to $0.7c$. The multiplicity of gray tracks in an event is denoted by n_g.

3. **Black tracks:** Black tracks predominantly originate from the slowly moving protons and other heavier fragments emitted by the excited target nucleus after an interaction has taken place. A proton generated black track may have kinetic energy < 30 MeV

and velocity $< 0.3c$. The ionization of the black tracks $I > 10I_0$ and their range < 3 mm in emulsion. The multiplicity of black tracks in an event is denoted by n_b.

4. **Projectile fragments:** The projectile fragments are a different class of tracks with constant ionization, long range and small emission angle. They remain confined within an extremely narrow forward cone of semi-vertex angle (θ_f), that depends on the momentum of the incoming nucleus. The tracks are very straight as they suffer very small Coulomb scattering. According to the Fermi gas model of nucleus, the Fermi energy of a nucleon is given by,

$$E_f = \frac{\hbar^2}{2m_p}\left(\frac{3}{2}\pi^2 n_p\right)^{2/3} \tag{2.25}$$

where m_p and n_p are, respectively the nucleon mass and nucleon number density. Numerically E_f is estimated to be 21 MeV and the corresponding Fermi momentum $p_f = \sqrt{2m_p E_f} \approx 200$ MeV/c. For an incident beam with $p_{lab} = 200A$ GeV/c, $\theta_f \approx$ a few mrad. The multiplicity of projectile fragments in an event is denoted by n_f.

The total number of heavy tracks (n_h) emitted from a primary ^{16}O-emulsion event is given by $n_h = n_b + n_g$. If in an event $n_h \geq 8$ with at least one heavy track with $Z \geq 2$, then it should be an interaction with a Ag/Br nucleus. In this investigation we have considered only those ^{16}O-AgBr events for which the projectile nuclei completely fragment in the collisions. The events have no projectile fragment of charge $Z \geq 2$. Only the shower tracks are used in this analysis. To avoid contamination, likely to arise from the fast moving protons, shower tracks falling within the forward Fermi cone as mentioned above, have been excluded from the scope of our analysis. Our final event samples consist of 280 ^{16}O-Ag/Br and 200 ^{32}S-Ag/Br events. The average shower track multiplicity for the ^{16}O-Ag/Br sample is $\langle n_s \rangle = 119.26 \pm 3.59$, whereas $\langle n_s \rangle = 217.79 \pm 6.16$ for the ^{32}S-Ag/Br sample.

2.6 Advantages and disadvantages of emulsion experiments

The nuclear emulsion is used simultaneously as a detector of charged particles and a target medium comprising of nuclei of varying mass numbers. As mentioned above, standard emulsions consist of H, C, N, O, Ag and Br nuclei. As far as high-energy interactions are concerned, information regarding target nucleus mass can be obtained from the characteristic structures of the heavy fragments in an event. Nuclear emulsion has the ability to detect all charged particles coming out of an event (also called a star), i.e. as a detector it has a 4π acceptance. Though, the detection efficiency is not equally good in all directions. Particularly along the vertical direction (toward or away from the direction of vision) the

efficiency is not good. Due to its high density the stopping power of nuclear emulsion is usually very high, and therefore, the interaction probability between a projectile particle and a target nucleus is also very large. Nuclear emulsions are light weight, very easy to handle and less costly compared to other detectors. The sensitivity of undeveloped nuclear emulsion plates lasts for a few weeks. Hence all charged particles passing through it are able to get their tracks permanently recorded for a reasonably long span of time. That makes nuclear emulsion a suitable detector for balloon flight and satellite experiments to study the cosmic-ray events, where heavy projectiles are seldom found. Neutral particles can also be indirectly detected in emulsions as and when they interact with the other nuclei, and produce tracks of charged particles. Nuclear emulsion can be used over a wide range of temperature, from the temperature of liquid Helium up to the boiling point of water. The most striking advantage of nuclear emulsion is its high spatial resolution. For horizontally irradiated stacks of emulsion pellicles an accuracy of 0.1 unit of pseudorapidity can be achieved. This unique feature makes the emulsion experiments important to investigate distributions of produced particles in narrow intervals of pseudorapidity.

There are some difficulties associated with the emulsion experiments too. It is not possible to identify the sign of a charged particle unless a magnetic field is applied. But it is also very difficult to get the magnetic field penetrate into the emulsion material, and to produce enough curvature in the track of a particle moving with relativistic speed. The sensitivity and thickness of emulsion pellicles are affected by temperature, humidity, age etc. Unless special care is taken these factors always introduce errors in the data. The track lengths of most of the produced particles in emulsion are at best a few mm. long. So high magnification devices such as high power microscopes are required to scan and collect the data. Even the automated devices could not speed up the scanning very significantly. This makes the data acquisition process a tedious and time consuming job. For AB interactions in the GeV range, where a few hundreds of particles may come out of an event, the time taken to build up even a moderate statistics requires huge effort. The collected data can never be made fully free from personal bias and errors. Measurement of momentum through elastic scattering is an even more tedious and time consuming process, making it almost impossible for any statistically significant number of tracks. Identification of the target fragments often becomes extremely difficult, and sometimes even impossible. However, a gross distinction between the light group (H, C, N, O) and the heavy group (Ag, Br) of target nuclei can be made.

2.7 Simulation

In this analysis we use the the Ultra-relativistic Quantum Molecular Dynamics (UrQMD) [20] model to simulate the experiment. UrQMD is a microscopic transport model where an AB interaction is considered as a superposition of many elementary NN interactions. UrQMD simulates the space-time evolution of an AB interaction, starting from its initial pre-equilibrium stage to the final freeze-out stage. At low and intermediate energies ($\sqrt{s_{NN}} < 5$ GeV) the model describes the phenomenology of hadronic interactions in terms of interactions between known hadrons and their resonances. At higher energies, typically at $\sqrt{s_{NN}} = 5$ GeV and above, the excitation of color strings and their subsequent fragmentation into hadrons are taken into account. The model was proposed mainly to give a microscopic description of the AB interactions. Until now there is no concrete theory of hadronic interactions, with their vastly different characteristics at different incident energies and in different kinematic regions. Perturbative quantum chromodynamics (pQCD) can be applied to describe hard processes where the four-momentum (Q^2) transfer is large. But pQCD is formally inappropriate for the description of soft processes (low-p_t physics) because of strong coupling. Therefore, low-p_t collisions are described in terms of phenomenological models. Now-a-days a variety of models for hadronic and nuclear collisions are available. The UrQMD is one of them which is quite appropriate for the collision energy involved in the present experiment.

The UrQMD is based upon covariant propagation of hadrons considered on the (quasi)particle level on classical trajectories in combination with stochastic binary scatterings, color string formation and resonance decays. It represents a Monte-Carlo solution of a large set of coupled partial integro-differential equations for the time evolution of various phase space densities of particle species like N, Δ, Λ, π etc. In this model nuclei are treated as a Fermi-gas with a Gaussian density distribution. The wave function of the nucleus is defined as the product of single nucleon Gaussian functions without invoking the Slater determinant that is necessary for proper anti-symmetrization of a many particle state. The nuclear (N-particle) wave function is given by,

$$\Phi = \prod_i \varphi_i(x_j, p_j, t) \tag{2.26}$$

Here a single particle wave function is

$$\varphi_j(x_j, p_j, t) = \left(\frac{2\alpha}{\pi}\right)^{3/4} \exp\left[-\alpha\left\{x_j - r_j(t)\right\}^2 + \frac{i}{\hbar} p_j(t) x_j\right] \tag{2.27}$$

In configuration space the centroids of the Gaussian function are distributed at random within a sphere of radius

$$R(A) = r_0 \left(\frac{1}{2} \left[A + (A^{1/3} - 1)^3 \right] \right)^{1/3} : \; r_0 = \left(\frac{3}{4\pi\rho_0} \right)^{1/3} \tag{2.28}$$

where ρ_0 is the nuclear matter density in the ground state. The finite width of these Gaussians result in a diffused surface region beyond the radius of that sphere. The initial momenta of the nucleons are chosen at random between 0 and local Thomas-Fermi momentum $p_f^{\max} = \hbar c(3\pi^2\rho)^{1/3}$, where ρ is the corresponding local nucleon density. A disadvantage of the initialization mentioned above is that the initialized nuclei are not really in their ground states with respect to the Hamiltonian used for their propagation. However, the parameters of the Hamiltonian are tuned to the equation of state for a finite sized nucleus and to the properties of finite nuclei. If however, the energy of the nucleons within the nucleus is minimized in a self consistent way, then the nucleus would collapse to a single point in momentum space because of the non-inclusion of Pauli's principle. One possible solution to this problem is the inclusion of fermionic properties of the nucleons via the antisymmetrization of the wave function of the nucleus. This ansatz has been implemented in the framework of the Fermionic Molecular Dynamics (FMD) [21]. But the FMD equations of motion are computationally very expensive. To get rid of the problems one can use the so called Pauli potential [22] in the Hamiltonian. Its advantage is that the initialized nuclei remain absolutely stable, whereas in the conventional initialization and propagation without the Pauli potential, the nuclei start evaporating single nucleons after $\approx 20 - 30$ fm/c. A drawback of such a potential is that the kinetic momenta of the nucleons are not equivalent to their canonical momenta, i.e. the nucleons carry the correct Fermi-momentum, but their velocities are zero. Furthermore, the Pauli potential leads to a wrong specific heat and changes the dynamics of string fragmentation.

For nuclear collisions the interaction potential used in UrQMD is the density dependent Skyrme potential [23]. This potential consists of a sum of a two and three-body interaction terms. The two-body term (E^{Sk2}) has a linear density dependence, and models the long-range attractive component of the NN interaction. Whereas the three-body term (E^{Sk3}) is responsible for the short-range repulsive part of the interaction. In addition to the Skyrme potential, the Yukawa (E^{Yuk}), the Coulomb (E^{Coul}) and the Pauli (E^{Pauli}) (optional) potentials are also included in UrQMD. In finite nuclei the usage of a Yukawa term has the advantage that the parameter can be tuned to the proper surface potential of the nuclei without changing the equation of state. With these interactions the classical

UrQMD Hamiltonian reads as,

$$H = \sum_{j=1}^{N} E_j^{kin} + \frac{1}{2}\sum_{j,k=1}^{N}\left(E_{jk}^{Sk2} + E_{jk}^{Yuk} + E_{jk}^{Coul} + E_{jk}^{Pauli}\right) + \frac{1}{6}\sum_{j,k,l=1}^{N} E_{jkl}^{Sk3} \tag{2.29}$$

The time evolution of the system is obtained by the requirement that the corresponding action is stationary under the allowed variation of the wave function. This yields an Euler-Lagrange equation for each parameter,

$$\dot{p_i} = -\frac{\partial\langle H\rangle}{\partial q_i} = -\nabla_{q_i}\sum_{j\neq i}\langle V_{ij}\rangle = -\nabla_{q_i}\langle H\rangle \tag{2.30}$$

$$\dot{q_i} = \frac{\partial\langle H\rangle}{\partial p_i} = \frac{p_i}{m} + \nabla_{p_i}\sum_{j}\langle V_{ij}\rangle = \nabla_{p_i}\langle H\rangle \tag{2.31}$$

The potential element is given by

$$\langle V_{ij}\rangle = \int d^3x_1 d^3x_2\, \varphi_i^*\varphi_j^*\, V(x_1,x_2)\, \varphi_i\varphi_j \tag{2.32}$$

These equations are solved numerically. Impact parameter of a collision is sampled according to the quadratic measure, $dW \sim bdb$. Two particles collide if their relative distance $d \leq d_0 = \sqrt{\sigma_{tot}/\pi}$. The total cross-section σ_{tot} depends on the center of mass energy $\sqrt{s_{NN}}$, the particle type and its isospin, which is taken to be symmetric. In the limit $\sqrt{s_{NN}} \geq 5$ GeV the CERN/HERA parametrization for the *pp* cross section is used [24]. Since the functional dependence of σ_{tot} on $\sqrt{s_{NN}}$ at low energies has a complicated shape, UrQMD uses a set of numerical values for that purpose.

Particle production in UrQMD either takes place via the decay of a meson or baryon resonance or via a string excitation and its fragmentation. For beam energies of about 10 GeV/nucleon particle production in UrQMD is dominated by resonance decays. Production cross-sections for the excitation of individual resonances can be calculated in the framework of one-pion exchange (OPE) or one-boson exchange (OBE) models [25]. Considering the number of resonances generated by the UrQMD, and the limited energy range of their applicability for cross section determination within OPE and OBE models, the calculation of all resonance excitation cross sections in the framework of these models is not practical. Therefore, an effective parametrization based on simple phase space considerations has been employed, and free parameters are tuned to experimental measurements. After the fragmentation, decay of the resonances proceeds according to the branching ratios compiled by the Particle Data Group [24]. The resonance decay products have isotropic distributions in the rest frame of the resonance. If a resonance is among the outgoing particles, its mass must be determined at first in accordance to the Breit-Wigner formula. If the resonance

decays into more than two particles, then the corresponding N-body phase space is used to calculate their momenta. If the outgoing phase space is occupied, the Pauli principle is applied to hadronic collisions. The collision term in UrQMD includes more than fifty baryon species (including nucleon, delta and hyperon resonances with masses up to 2.25 GeV) and five meson nonets (including strange meson resonances). The particles are supplemented by their corresponding anti-particles and all isospin-projected states. The states can either be produced in string decays, s-channel collisions or resonance decays. For excitations with masses more than 2 GeV, a string picture is used. Full baryon/antibaryon symmetry is included in the UrQMD model.

2.7.1 Modeling Bose-Einstein correlation

The Bose-Einstein correlation (BEC) is one of the primary reasons of observing particle correlations in relativistic nuclear collisions. The BEC between identical mesons is a quantum statistical effect that is not present in the UrQMD model. We know that intensity correlations appear due to the symmetrization of the two-particle states. Accordingly, any two particles having momenta q_1 and q_2, can form a state with amplitude

$$\tilde{A} \propto \frac{1}{\sqrt{2}} \left[e^{i(q_1 x_1 + q_2 x_2)} + e^{i(q_1 x_2 + q_2 x_1)} \right] \tag{2.33}$$

where x_i ($i = 1, 2$) is the emission point of the i-th particle. If the particles are emitted incoherently, the observed two-particle spectrum is expressed in terms of single particle density function $\rho(p)$ as,

$$\rho_2(q_1, q_2) \propto \int dx_1 \rho_1(x_1) \int dx_2 \rho_1(x_2) |\tilde{A}(q_1, q_2)|^2 \tag{2.34}$$

and the two-particle intensity correlation function is given by,

$$C_2(Q) = \frac{\rho_2(q_1, q_2)}{\rho_1(q_1)\rho_1(q_2)} = 1 \pm |R(Q)|^2 \tag{2.35}$$

where the sign $+(-)$ corresponds to bosons (fermions) and $R(Q)$ is the normalized Fourier transform of ρ, the source density [26]

$$R(Q) = \frac{\int dx\, \rho(x) e^{i(q_1 - q_2)x}}{\int dx\, \rho(x)} \tag{2.36}$$

This quantity is often parametrized in terms of a source radius R_{inv}, related to the size of the emission region, and a chaoticity parameter λ, which measures the strength of the effect.

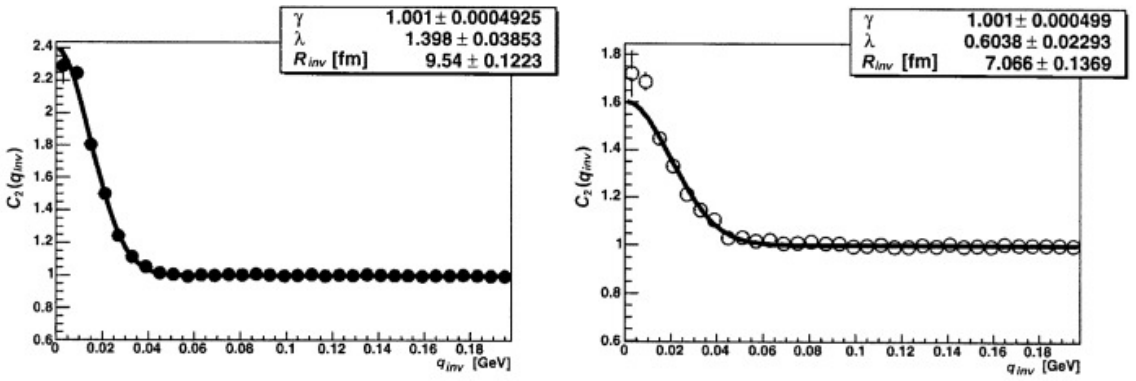

Figure 2.2: The Bose-Einstein correlation function $C_2(Q = q_{\rm inv})$ for $\pi^-\pi^-$ pairs using the charge reassignment algorithm (left panel) and the weighting method (right panel). Gaussian fits are shown in each diagram. The figure is taken from ref. [32]

From the above equation one derives,

$$|R(Q)|^2 = \lambda e^{-R_{inv}^2 Q^2} \tag{2.37}$$

after assuming a spherical emission volume with a Gaussian density distribution. The study of BEC among identical meson pairs is carried out by using the ratio of correlation obtained from the data to the same obtained from a Monte-Carlo (MC). The common method of introducing BEC among particles generated via classical MC simulations is the weighting method with a two-boson weight factor,

$$f_{BEC}(q_{\rm inv}, x) = 1 + \cos[(q_1 - q_2).(x_1 - x_2)] \tag{2.38}$$

The weighting method computes f_{BEC} using particle momenta and coordinates at the freeze-out. A drawback of this method is that it cannot simulate multi-boson correlations. However, with transport models the weighting method is well justified, as the phase-space densities generated by the transport models are rather low. Recently, a new algorithm has been suggested [27], which claims to overcome this limitation. The algorithm is based on reassigning charges of produced pions and results in formation of quantum Bose-Einstein cells in phase-space, in which the number of identical bosons is enhanced. It conserves the energy-momenta and does not alter any single particle inclusive distribution. Since its original study [28], the BEC of various particle pairs has been studied for a large variety of interacting systems over a wide range of energies [29, 30]. It has been observed that like-charge particle correlations are much stronger than those between unlike-charge particles [31]. We include the BEC effect numerically in the form of an *after burner* [27] making use of the output of the event generator. As mentioned, the algorithm is based on the reassignment of electrical charges of particles, while keeping the particle coordinates unaltered. The particle information are contained in the UrQMD output file *test.f19* written in the OSCAR

format. Only the (event-wise) pi-mesons are taken from the output file. Each particle entry in an event contains a serial number, the particle ID, the particle freeze-out 4-momenta (p_x, p_y, p_z, E), the particle mass m, and the final freeze-out 4-coordinates (x, y, z, t). The steps followed in the charge reassignment algorithm are listed below.

(i) Choose a meson at random from an event, call it the i-th one, and assign a charge 'sign' i.e., $+$, $-$ or 0 to it, irrespective of its original charge, with weight factors respectively given by $p_+ = n_+/n$, $p_- = n_-/n$ and $p_0 = n_0/n$. Here n_+, n_-, n_0 are, respectively the number of $+ve$, $-ve$ and neutral mesons in the event, and $n(= n_+ + n_- + n_0)$ is the total number of mesons present in that event. The chosen meson, i.e. the i-th one, defines a phase space cell.

(ii) Calculate the distances in 4-momenta $\delta_{ij}(p) = |p_i - p_j|$, and 4-coordinates $\delta_{ij}(x) = |x_i - x_j|$ between the already chosen meson (the i-th one) and all other mesons (indexed by j) that are not yet assigned any charge sign.

(iii) Assign a weight factor

$$P_{ij} = \exp\left[-\frac{1}{2}\,\delta_{ij}^2(p)\,\delta_{ij}^2(x)\right] \tag{2.39}$$

to each of the j-th particles. The weight factor actually characterizes the bunching probability of the particles in a given cell.

(iv) Then start generating uniformly distributed random numbers $r \in (0, +1)$. If $r < P_{ij}$, reassign to the j-th meson the same charge sign as the i-th one. Continue the process until either r exceeds P_{ij}, or until all mesons in the event having the same charge sign as the i-th one are exhausted.

(v) Repeat the whole set of operations for all other mesons for which the charge reassignment has not yet been done. Obviously, the weight factors $p_\pm$ and p_0 will now be modified, as some of the particles present in the event are already used up. The algorithm is repeated until the mesons belonging to all charge varieties in the event are used up.

The UrQMD model provides all pion pairs with $Q^2 = (p_i - p_j)^2 = (\Delta E)^2 - (\delta p)^2 < 0$. In order to keep the value of the factor (P_{ij}) below unity, only the pion pairs having a space-like separation, $-R^2 = (x_i - x_j)^2 = (\Delta t)^2 - (\Delta x)^2 < 0$ are accepted [32]. Without changing the overall set of 4-momenta, 4-coordinates, or total meson charge of the system, we can in this way generate clusters of identical charge states of mesons. In Figure 2.2 we illustrate the correlation function $C_2(Q = q_{inv})$ for $\pi^-\pi^-$ pairs computed from the charge reassignment procedure (left panel) and the weighting procedure (right panel) for Au+Au interactions at $\sqrt{s_{NN}} = 200$ GeV generated by the UrQMD model. The results complement each other.

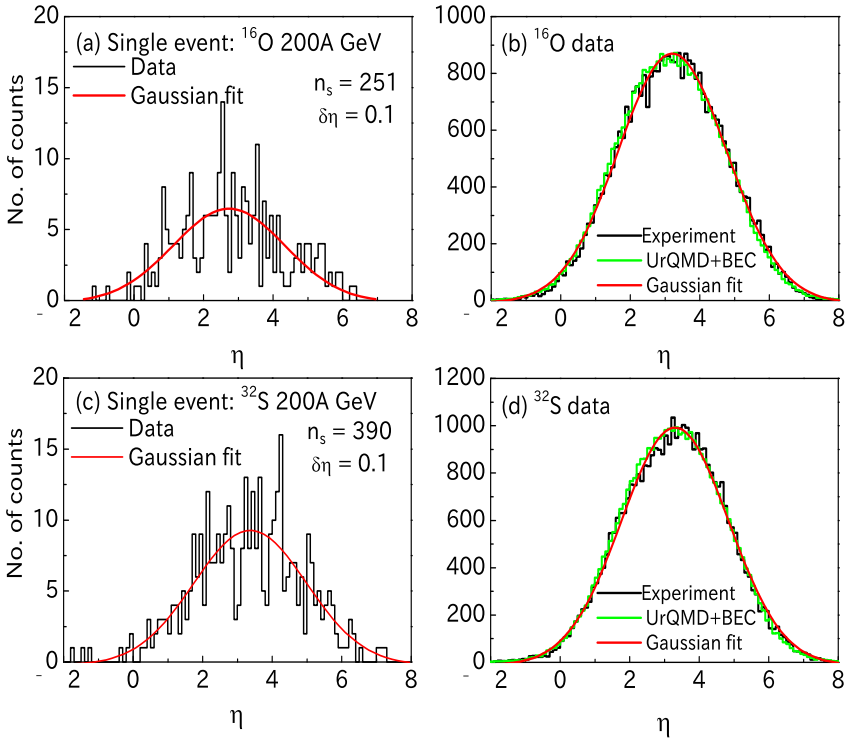

Figure 2.3: (a) η-distribution for an event in ^{16}O-Ag/Br interaction. (b) η-distribution for the ^{16}O sample compared with the UrQMD+BEC model simulation. The lower panel is same as in the upper panel but for the ^{32}S data. In all the cases the experimental distributions are fitted by a Gaussian distribution.

2.7.2 Sampling the simulated events

Using the UrQMD code we simulate the ^{16}O-Ag/Br and ^{32}S-Ag/Br events at $p_{\rm lab} = 200A$ GeV/c. We first generate minimum bias samples in the laboratory frame separately for the Ag and Br targets and for each projectile. These independent event samples corresponding to Ag and Br targets are then mixed up at random to generate a minimum bias event samples on ^{16}O-Ag/Br and ^{32}S-Ag/Br interactions. The proportional abundance of Ag and Br nuclei in G5 emulsion [13] is maintained during the mixing procedure. All newly produced mesons in the simulated events are retained in the respective output files. The event samples are then passed through the charge reassignment algorithm described in the previous section. From each minimum bias sample we select such events as to match the corresponding experimental shower track multiplicity distribution. Obviously the average shower track multiplicity of the simulated sample is same as the experimental one. The event sample simulated for each projectile is five times as large as that of the experiment. The UrQMD simulation that includes the BEC is denoted by UrQMD+BEC in this document.

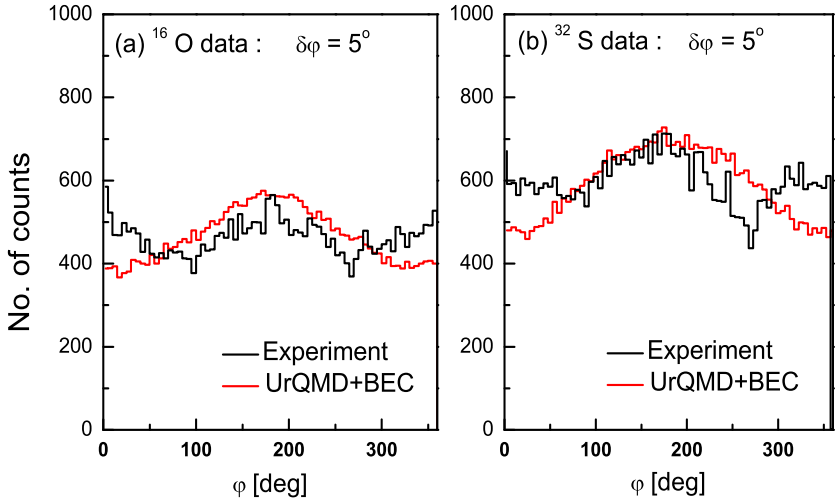

Figure 2.4: Distributions of φ (a) for ^{16}O-Ag/Br and (b) for ^{32}S-Ag/Br interactions. The UrQMD+BEC simulations are shown with the experiments.

2.8 Basic distributions

By measuring the emission angle θ of a shower track with respect to the projectile track the pseudorapidity variable of a particle is determined,

$$\eta = -\ln\ [\tan(\theta/2)] \tag{2.40}$$

The resolution in η is

$$\delta\eta = -\frac{1}{\sin\theta}\,\delta\theta \tag{2.41}$$

Therefore, at small angles only a small error in θ ensures a good resolution in η. The accuracy of our η-measurement is $\delta\eta \approx 0.1$ unit. In a 1-dimensional analysis we take η as the basic variable, while it is the (η, φ) plane for a 2-dimensional analysis.

In Figure 2.3 the η-distributions of the shower tracks for two individual events, as well as those for the ^{16}O-Ag/Br and ^{32}S-Ag/Br event samples are shown. The η-distribution of shower tracks for a single event has a lot of spikes and valleys, apparently devoid of any fixed pattern. The background of such event-wise distributions can be very roughly approximated by Gaussian curves, as shown in the figure. For a large sample of events these fluctuations are however smoothed out. The event averaged η-distributions for both projectiles can also be described by Gaussian functions. We fit Gaussian curves to the data and obtain the following fit parameters. The centroid $\eta_0 = 3.32 \pm 0.01$, the peak density ${N_{\rm ev}}^{-1}\, dn_s/d\eta|_{\eta_0} = 31.19 \pm 0.11$, and the width $\sigma_\eta = 1.55 \pm 0.01$ for the ^{16}O-Ag/Br sample. Corresponding values for For the ^{32}S-Ag/Br sample are, $\eta_0 = 3.37 \pm 0.01$, ${N_{\rm ev}}^{-1}\, dn_s/d\eta|_{\eta_0} = 56.34 \pm 0.24$ and $\sigma_\eta = 1.55 \pm 0.01$. In these diagrams of we have included the η-distributions of charged hadrons obtained from the UrQMD generated ^{16}O-Ag/Br and ^{32}S-Ag/Br events, where as

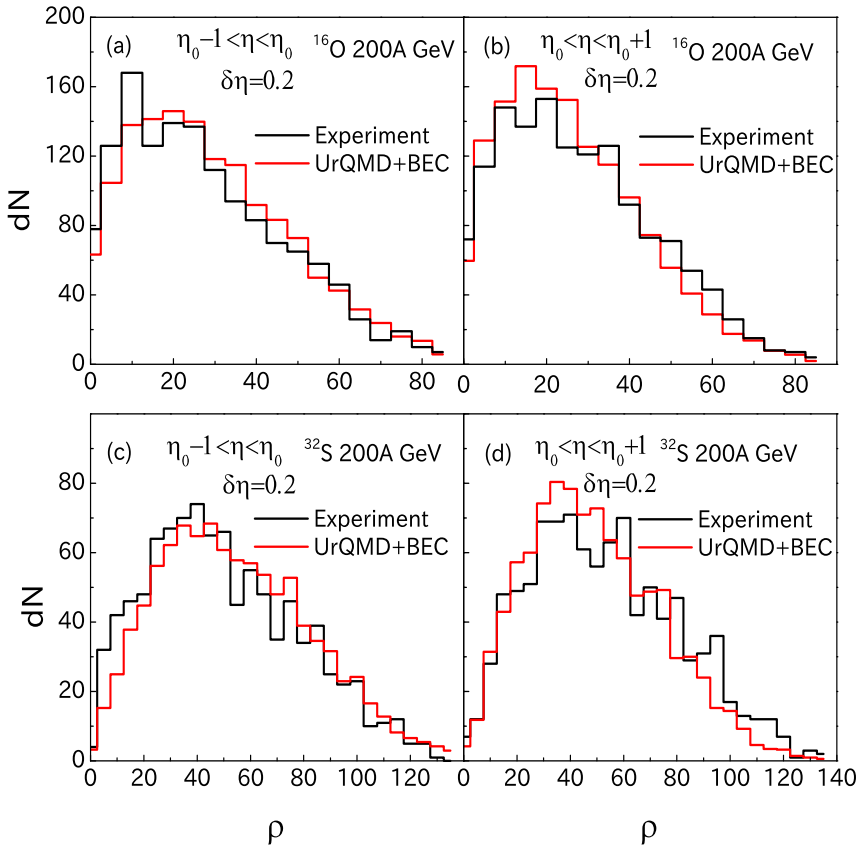

Figure 2.5: Distributions of local pseudorapidity density of shower tracks for ^{16}O-Ag/Br (Figure (a, b)) and ^{32}S-Ag/Br (Figure (c, d)) interaction at 200A GeV/c. Two region is chosen for distribution, $\eta_0 - 1 < \eta < \eta_0$ and $\eta_0 < \eta < \eta_0 + 1$ for $\delta\eta$=0.2.

mentioned in section 2.7, the BEC has been mimicked as an after burner to the simulated data through a charge reassignment algorithm. Following Bjorken's hydrodynamical model [33] one can calculate the initial energy density (ϵ) for each event sample by using the peak density of the particles,

$$\epsilon = \frac{m_t}{\tau\,\widehat{A}}\;\frac{d\langle n_{all}\rangle}{d\eta}\bigg|_{\eta=\eta_0} \tag{2.42}$$

where ϵ is averaged over the transverse area $\widehat{A}$, and where τ the proper time in which the matter present within the collision volume should equilibrate. We consider $n_{all} = 1.5\,n_s$, assuming equal abundance of all three charge species $(\pm 1e, 0)$. We set the transverse mass of a pion at $\langle m_t\rangle = 0.38$ GeV, choose $\tau = 1$ fm/c, assume that $\widehat{A}$ is roughly the geometrical cross-sectional area of the ^{16}O-nucleus, and replace $\frac{d\langle n_{all}\rangle}{d\eta}|_{\eta=\eta_0}$ by $1.5\rho_0$. The initial energy density values come out as $\epsilon \approx 0.82$ GeV/fm^3 in ^{16}O-Ag/Br interaction and $\epsilon \approx 0.92$ GeV/fm^3 in ^{32}S-Ag/Br interaction. We note that these ϵ-values are just below the threshold mark (ϵ = a few GeV/fm^3) needed for the QGP formation in AB collisions. The azimuthal angle (φ) distributions of shower tracks are shown in Figure 2.4. We see that the φ-distributions have dips around $\varphi = 90^0$ and 270^0. Most probable reasons of such azimuthal

asymmetries are, (i) inefficient recording of the shower tracks directly toward or away from the direction of vision, and (ii) the collective flow of charged hadrons. The UrQMD+BEC generated distributions are plotted together with the respective experiment. The distributions of shower track density values in the central particle producing regions, ($\rho = dn_s/d\eta$) for our ^{16}O-Ag/Br and ^{32}S-Ag/Br data samples are shown in Figure 2.5 (a) (left panel) $(\eta_0 - 1) < \eta < \eta_0$ and (b) (right panel) $\eta_0 < \eta < (\eta_0 + 1)$. The UrQMD+BEC simulated distributions are incorporated in these diagrams too. The distributions are asymmetric and each simulation can more or less reproduce the corresponding experiment. Particle densities $3-4$ times as large as the most probable density value are observed both in the experiments and in the simulations. In the following chapters we are going to investigate the small scale structures of these high-valued density fluctuations.

Bibliography

[1] C. F. Powell, P. H. Fowler and D. H. Perkins, The study of elementary particles by photographic method, Pergamon, Oxford (1959).

[2] A. E. S. Green, Nuclear Physics, McGraw-Hill Book Company (1955).

[3] L. Voyvodic, Bristol Conf. Rep. Dec. (1951).

[4] L. Voyvodic and E. Pickup, Phys. Rev. 85, 91 (1952).

[5] A. H. Morrish, Phil. Mag. 43, 533 (1952).

[6] R. R. Daniel, J. H. Davis, J. H. Mulvay and D. H. Perkins, Phil. Mag. 43, 753 (1952).

[7] R. M. Sternheimer, Phys. Rev. 89, 1148 (1953).

[8] C. O'Ceallaigh, Phil. Mag. 42, 1032 (1951).

[9] P. H. Fowler and D. H. Perkins, Phil. Mag. 46, 587 (1955).

[10] N. F. Mott, Proc. Roy. Soc. (London), 124, 425 (1929).

[11] B. Rossi, High Energy Particles, Prentice Hall, Englewood Chiffs, New Jersey (1952).

[12] C. M. G. Lattes *et al.,* Proc. Phys. Soc. (London) 61, 173 (1948).

[13] W. H. Barkas, Nuclear Research Emulsions, Vols. I & II, Academic Press (1963).

[14] P. Freier, E. J. Lofgren, E. P. Ney and F. Oppenheimer, Phys. Rev. 74, 1818 (1948).

[15] E. J. Williams, Phys. Rev. 58, 292 (1940).

[16] P. H. Fowler, Phil. Mag. 41, 169 (1950).

[17] J. Thomas and P. Jacobs, High Energy Heavy Ion Experiments, Eleventh International Conference on Ultra-Relativistic Nucleus-Nucleus Collisions, 9-13 January 1995, Quark Matter '95, p. 28-29, Monterey, California, USA.

[18] G. Singh and P. L. Jain, Z. Phys. A 344, 73 (1992).

[19] M. K. Ghosh, Some Aspects of Multiparticle Production in ^{32}S-Ag/Br Interactions at 200A GeV/c (Ph.D. Thesis, North Bengal University, 2008).

[20] S. A. Bass *et al.*, Prog. Nucl. Part. Phys. 41, 255 (1998);
M. Bleicher *et al.*, J. Phys. G 25, 1859 (1999).

[21] H. Feldmeier, Nucl. Phys. A 515, 147 (1990).

[22] L. Wilets *et al.*, Nucl. Phys. A 282, 341 (1977).

[23] T. H. R. Skyrme, Nucl. Phys. 9, 615 (1959).

[24] R. Barnett *et al.*, Phys. Rev. D 54, 1 (1996).

[25] M. Berenguer (Ph.D. Thesis, Goethe University, Frankfurt am Main, Germany, 1993).

[26] M. G. Bowler, Z. Phys. C 29, 617 (1985).

[27] O. V. Utyuzh, G. Wilk and Z. Wlodarczyk, Phys. Lett. B 522, 273 (2001).

[28] G. Goldhaber *et al.*, Phys. Rev. Lett. 3, 181 (1959) ; Phys. Rev. 120, 300 (1960).

[29] E. A. Wolf, Proc. XXVII, Int. Conf. High Energy Physics, Glasgow, Eds. P. J. Bussy and I. J. Knowles, p.1281 (1994).

[30] G. Alexander, I. Cohen and E. Levin, Phys. Lett. B 452, 159 (1999).

[31] A. D. Angelis, Mod. Phys. Lett. A 5, 2395 (1990).

[32] M. Bystersky, Nucleonica Supplement, 49, s37 (2004).

[33] J. D. Bjorken, Phys. Rev. D 27, 140 (1983).